Memorias del 2023 Congreso Nacional de Control Automático
25-27 de Octubre, 2023. Acapulco, Guerrero, México.

Real-Time Control of Underactuated Systems in a Mechatronics Kit via a Novel LMI-Based Sliding Mode Approach ⋆

César Calvo * **David Vázquez** * **Miguel Bernal** *

* *Dept. of Electrical and Electronics Engineering, Sonora Institute of Technology, 5 de Febrero 818 Sur, 85000, Obregon City, Mexico (e-mail: miguel.bernal@itson.edu.mx).*

Abstract: Real-time implementation of a sliding mode control scheme based on the unit vector approach, for a variety of underactuated configurations of a mechatronics kit (rotational, inertia, and double pendulum) is presented in this work. Details are given to perform diffeomorphisms leading to the required normal form, based on which design conditions are cast as linear matrix inequalities, thus improving numerical systematicness of the traditional methodology. Once the control law is designed, its implementation requires reliable estimates of the velocities since the different plants under consideration do not measure them; to this end, Levant's robust differentiator is employed. Results are provided that show the effectiveness of the proposal.

Keywords: Sliding Mode, Unit Vector Approach, Levant Differentiator, Underactuated System, Normal Form, Linear Matrix Inequality

1. INTRODUCTION

Standard sliding mode control is a well-established methodology characterized by its insensitivity to matched disturbances and finite-time onset of a reduced-order dynamics known as sliding motion (Edwards and Spurgeon, 1998). Among the different 1st-order sliding mode control schemes we can find robust eigenstructure assignment (Lee and Yang, 2009), continuous approximations (Fliegner and Smith, 1998), and the unit vector approach (Ryan and Corless, 1984). The latter methodology is apt for multi-input multi-output (MIMO) systems provided the sliding surface $s(t)$ (the manifold to which the system will be restricted to during sliding motion) is of the same dimension as the control input $u(t)$, i.e., $s \in \mathbb{R}^m$, $u \in \mathbb{R}^m$. Despite this restriction, the unit vector approach has proved to be an effective control tool for a variety of applications (Ashari, 2004; Capriotti and Marti-Renom, 2008; Hajkarami et al., 2010). Since this work is real-time oriented, the referred methodology serves as the starting point for our proposal.

Control schemes are better tested when applied to underactuated systems with rapid dynamics; this is the reason behind the repeated use of a varieties of pendulums to illustrate a control law effectiveness. Examples of such schemes are the inverted pendulum on a cart (Angeli, 2001), the double pendulum also known as the Pendubot (Begovich et al., 2002), the 3-link SISO system (Farwig et al., 1990), the pendulum on an inclined rail (Furuta et al., 1980), the inertia wheel link (Spong et al., 2001), and the rotational (also known as Furuta) pendulum (Furuta et al., 1992). The Mechatronics Kit by Quanser (Quanser, 2006) allows configuring the plant as a Pendubot, an inertia, or Furuta pendulum. The proposal in this work is put at test both in simulation and real-time for all these plants.

Certainly, applying sliding mode control schemes to the aforementioned plants is not novel: in Izutsu et al. (2008); Wadi et al. (2018); Xu et al. (2020) they are applied to the Furuta pendulum; in Hernández (2003); Khalid and Memon (2014); Sun et al. (2015) the inertia pendulum is controlled with a variety of sliding mode schemes; they have also been successfully applied to the Pendubot in Van Kien et al. (2016); Yoo (2013); Zehar and Benmahammed (2013). However, none of these schemes has been developed with numerically implementable methodologies, i.e., they rely on the designer ability to tune controller parameters, Lyapunov functions or gains. In contrast, our proposal is based on linear matrix inequalities (LMIs) (Boyd et al., 1994), which can be solved in polynomial time by means of efficient algorithms already implemented in commercially available software (Gahinet et al., 1995); bounds on the different terms are not needed as positions (angle) are considered available via encoders and angular velocities are exactly reproduced in finite time via Levant's robust differentiators Levant (2003).

⋆ This project has been supported by the CONACYT scholarship 758980 and the ITSON PROFAPI_CA_2023_002.

The paper is organized as follows: since the proposal is based on the unit vector approach and this requires the system to be put in a normal form, these preliminaries are presented in Section 2 along with the Levant's robust differentiator which will be later employed to estimate angular velocities; Section 3 has a first part where the main theoretical contribution is made, i.e., a novel LMI-based sliding mode unit vector approach; then, based on it, specific control laws are developed for each of the 3 plants under consideration; these control laws are put at test in Section 4, both in simulation and real-time implementation; finally, some concluding remarks are made in Section 5.

2. PRELIMINARIES

This section has three parts: a description of the procedure leading to the normal form of the nonlinear systems under consideration, the unit vector approach for sliding mode control based on a reformulation of the normal form, and the basics on Levant's robust differentiator.

2.1 Normal form

The nonlinear models of the different underactuated plants in the mechatronics kit (inertia, double and rotational pendulums) are all 4-state (2 positions and 2 velocities) 1-input systems (Quanser, 2006), i.e.,

$$\dot{x} = f(x) + g(x)u,\ y = h(x),\ x \in \mathbb{R}^4,\ u \in \mathbb{R}. \quad (1)$$

The underactuated position of all these plants can be viewed as an output $y = h(x)$, $y \in \mathbb{R}$; in all of these cases, the relative degree of such output is 2. Thus, a (possibly local) diffeomorphism $z = T(x)$, $T(0) = 0$,

$$z \equiv \begin{bmatrix}\eta_1\\ \eta_2\\ \xi_1\\ \xi_2\end{bmatrix} = \begin{bmatrix}\phi_1(x)\\ \phi_2(x)\\ h(x)\\ L_f h(x)\end{bmatrix} \equiv T(x), \quad (2)$$

such that $(\partial\phi_i/\partial x)g(x) = 0$ for $i \in \{1, 2\}$, $L_f h(x) \equiv (\partial h/\partial x)f(x)$, can be found (Khalil, 2014, Section 8.1), allowing to write (1) as

$$\dot{z}_1(t) = A_{11}z_1(t) + A_{12}z_2(t) + f_u(z) \quad (3)$$
$$\dot{z}_2(t) = A_{21}z_1(t) + A_{22}z_2(t) + B_2u(t) + f_m(z, u), \quad (4)$$

where $z_1 \equiv [\eta_1\ \eta_2\ \xi_1]^T$, $z_2 \equiv \xi_2$, $A_{11} \in \mathbb{R}^{3\times3}$, $A_{12} \in \mathbb{R}^{3\times1}$, $A_{21} \in \mathbb{R}^{1\times3}$, $A_{22} \in \mathbb{R}$, $B_2 \in \mathbb{R}$ are arbitrary constant matrices, and $f_u(\cdot) : \mathbb{R}^4 \to \mathbb{R}^3$, $f_m(\cdot) : \mathbb{R}^4 \to \mathbb{R}$, hold

$$\begin{bmatrix}f_u(z)\\ f_m(z,u)\end{bmatrix} = \frac{\partial T}{\partial x}(f(x)+g(x)u)\bigg|_{x=T^{-1}(z)} - \begin{bmatrix}A_{11} & A_{12}\\ A_{21} & A_{22}\end{bmatrix}\begin{bmatrix}z_1\\ z_2\end{bmatrix} - \begin{bmatrix}0\\ B_2\end{bmatrix}u.$$

2.2 Unit vector approach

Sliding mode control does not require the specific form of the nonlinear terms as long as they are bounded; this is the reason it can also handle time-varying terms in the same framework. The unit vector approach in (Edwards and Spurgeon, 1998, Section 3.6) adopts this point of view for systems of the form (3)-(4), assuming that $\|f_u(z)\| \le k_1\|z\| + k_2$, $\|f_m(z, u)\| \le k_3\|u\| + \alpha(z)$, for some $k_1, k_2, k_3 \ge 0$, based on which the following result, summarizing several sections in the referred work, can be stated:

Theorem 1. The equilibrium point $z = 0$ of the closed-loop system resulting from substitution of $u(t) = u_l(t) + u_{nl}(t)$ in (3)-(4) where

$$u_l = \Lambda^{-1}\left(-S_2\bar{A}_{21}z_1 - (S_2\bar{A}_{22}S_2^{-1} - \Phi)s(t)\right), \quad (5)$$

$$u_{nl} = -\rho(z)\Lambda^{-1}\frac{P_2 s(t)}{\|P_2 s(t)\|}, \quad s(t) \neq 0, \quad (6)$$

with $\bar{A}_{11} = A_{11} - A_{12}M$, $\bar{A}_{21} = M\bar{A}_{11} + A_{21} - A_{22}M$, $\bar{A}_{22} = MA_{12} + A_{22}$, $P_2 > 0$, $P_2\Phi + \Phi^T P_2 = -1$, $s(t) = S_2Mz_1(t) + S_2z_2(t)$, $\Lambda = S_2B_2$, $\det(\Lambda) \neq 0$, $k_3\kappa(\Lambda)\|B_2^{-1}\| < 1$, $\sigma(A_{11} - A_{12}M) \in \mathbb{C}^-$, and

$$\rho(z) = \frac{\|S_2\|\left(\|M\|\left(k_1\|z\| + k_2\right) + k_3\|u_l\| + \alpha(z)\right) + \gamma_2}{1 - k_3\kappa(\Lambda)\|B_2^{-1}\|},$$

for some $\gamma_2 > 0$, $\Phi \in \mathbb{R}$, $P_2 \in \mathbb{R}$, $S_2 \in \mathbb{R}$, $M \in \mathbb{R}^{1\times3}$, $\Lambda \in \mathbb{R}$, is asymptotically stable. Moreover, the sliding surface $s = 0$ is reached in finite-time.

Proof. The proof can be found in (Edwards and Spurgeon, 1998, Section 3.6).

2.3 Levant's robust differentiator

Real-time implementation of our proposal has to deal with the fact that only positions are available via encoders; velocities will be obtained via a finite-time convergent Levant's robust differentiator (Levant, 2003):

Theorem 2. If the parameters $\lambda_i > 0$, $i \in \{0, 1, \ldots, o\}$, in

$$\begin{aligned}
\dot{v}_0 &= -\lambda_0\left|v_0 - f(t)\right|^{\frac{o}{o+1}}\operatorname{sign}\left(v_0 - f(t)\right) + v_1\\
\dot{v}_1 &= -\lambda_1\left|v_1 - v_0\right|^{\frac{o-1}{o}}\operatorname{sign}\left(v_1 - v_0\right) + v_2\\
&\vdots\\
\dot{v}_{o-1} &= -\lambda_{o-1}\left|v_{o-1} - v_{o-2}\right|^{\frac{1}{2}}\operatorname{sign}\left(v_{o-1} - v_{o-2}\right) + v_o\\
\dot{v}_o &= -\lambda_o\operatorname{sign}\left(v_o - v_{o-1}\right),
\end{aligned} \quad (7)$$

are properly chosen, then $v_i = f^{(i)}(t)$, $i \in \{0, 1, \ldots, o\}$, in the absence of input noises after a finite time of a transient process.

Proof. The proof can be found in (Levant, 2003, Section 5).

System (7) is an o-th order Levant's robust differentiator, $o \ge 1$; although it will be employed only to obtain the first derivative of a state. It is important to notice that the accuracy of such derivative estimation increases as o is augmented. To this end, it is advised to choose $\lambda_0 > 0$ and $\lambda_i > L$, $i \in \{1, 2, \ldots, o\}$, with $L > 0$ being a Lipschitz constant for $f'(t)$.

3. CONTROL LAW DEVELOPMENTS

Theorem 1 summarizes several design conditions in (Edwards and Spurgeon, 1998, Section 3.6), but none of them

is either LMI-based nor adapted to the specific characteristics of the plants in the mechatronics kit. Figure 1 shows the different parts of our proposal: for each plant, the control scheme employs a pair of Levant's robust differentiators (7) to estimate the system velocities; both positions and estimated velocities enter the control block which is split in two parts: on the one hand, an off-line calculation of the normal form and some gains that are obtained via novel LMI conditions; on the other hand, an on-line implementation of the unit vector sliding mode control based on the different off-line elements.

The following is a novel LMI formulation of the unit vector approach which also takes into account the fact that the nonlinear models of the mechatronics kit plants are known, thus allowing to express some bounds by simply taking norms of known expressions.

Theorem 3. The equilibrium point $z = 0$ of the closed-loop system resulting from substitution of $u(t) = u_l(t) + u_{nl}(t)$ in (3)-(4) with

$$u_l = \Lambda^{-1}\left(-S_2\bar{A}_{21}z_1 - (S_2\bar{A}_{22}S_2^{-1} - \Phi)s(t)\right), \quad (8)$$

$$u_{nl} = -\rho(z)\Lambda^{-1}\frac{P_2 s(t)}{\|P_2 s(t)\|}, \quad s(t) \neq 0, \quad (9)$$

where the LMIs

$$P_2 > 0,\ P_2\Phi + \Phi^T P_2 < 0, \quad (10)$$

$$X_1 > 0,\ A_{11}X_1 - A_{12}N + X_1^T A_{11}^T - N^T A_{12}^T < 0, \quad (11)$$

are solved for decision variables $P_2 \in \mathbb{R}$, $X_1 \in \mathbb{R}^{3\times 3}$, and $N \in \mathbb{R}^{1\times 3}$, with $M = NX_1^{-1}$, $\bar{A}_{11} = A_{11} - A_{12}M$, $\bar{A}_{21} = M\bar{A}_{11} + A_{21} - A_{22}M$, $\bar{A}_{22} = MA_{12} + A_{22}$, $s(t) = S_2Mz_1(t) + S_2z_2(t)$, $S_2 = \Lambda B_2^{-1}$, and

$$\rho(z) \geq \frac{\|S_2\|\left(\|M\|\|f_u(z)\| + \left\|f_m(z,u) - \frac{\partial f_m}{\partial u}u\right\| + \left\|\frac{\partial f_m}{\partial u}\right\|\bar{u}\right) + \gamma_2}{1 - \left\|\frac{\partial f_m}{\partial u}\right\|\kappa(\Lambda)\|B_2^{-1}\|}, \quad (12)$$

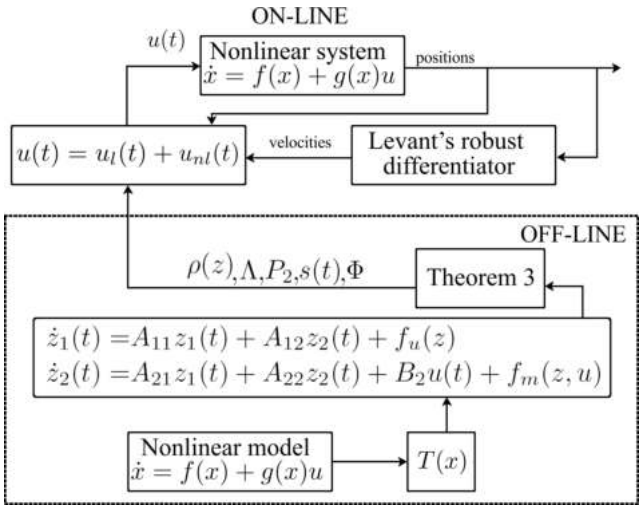

Fig. 1. Proposed control scheme.

for some $\gamma_2 > 0$, $\Phi < 0$, $\Lambda \in \mathbb{R}$ such that $\det(\Lambda) \neq 0$ and $\|\partial f_m/\partial u\|\,\kappa(\Lambda)\|B_2^{-1}\| < 1$, is asymptotically stable.

Proof. LMI condition (10) guarantees the expression $P_2\Phi + \Phi^T P_2$ is negative-definite, which is required for $V(s) = s^T P_2 s$ to be a Lyapunov function establishing attractiveness of the sliding surface (see (Edwards and Spurgeon, 1998, Section 3.6.1)); LMI condition (11) guarantees a stable sliding motion since it makes the pair (A_{11}, A_{12}) stable by means of the gain M (see (Bernal et al., 2022, Section 5.2)). Recall that the systems under consideration are not uncertain; this means that $f_u(z)$ and $f_m(z,u)$ are known and available (up to a finite-time transient to obtain the velocities by means of the Levant's robust differentiator), which means that their norms can be readily used instead of former bounds $k_1\|z\| + k_2$ and $k_3\|u\| + \alpha(z)$, respectively, provided some adjustments are made to avoid an algebraic loop on u for $\|f_m(z,u)\|$. This adjustment is as follows: since $f_m(z,u) = f_m(z,u) - (\partial f_m/\partial u)u + (\partial f_m/\partial u)u$, this means that, for a given bound of the input $\|u\| \leq \bar{u}$, we have:

$$\begin{aligned}\|f_m(z,u)\| \leq& \|f_m(z,u) - (\partial f_m/\partial u)u\| + \|(\partial f_m/\partial u)u\| \\ \leq& \|f_m(z,u) - (\partial f_m/\partial u)u\| + \|(\partial f_m/\partial u)\|\bar{u},\end{aligned}$$

which completes the substitution made on (12), thus concluding the proof. □

Remark 4. Two of the configurations of the mechatronics kit have a constant value multiplied by the input u in the last equation of the normal form (4); this implies that $f_m(\cdot)$ depends exclusively on z and therefore, since $\partial f_m/\partial u = 0$, $\rho(z)$, in can be used directly

$$\rho(z) \geq \|S_2\|\left(\|M\|\|f_u(z)\| + \|f_m(z)\|\right) + \gamma_2. \quad (13)$$

The specific transformations leading to the normal form (3)-(4) for each configuration of the mechatronics kit are now presented. Once this form is obtained, applying Theorem 3 will be straightforward.

3.1 Inertia pendulum

The inertia pendulum consists of a free arm linked to a fixed frame by one end, with a DC motor on the other end; its mathematical model has the form (1) with

$$f(x) = \begin{bmatrix} x_2 \\ gc\sin(x_1 - \pi)/a \\ x_4 \\ -gc\sin(x_1 - \pi)/a \end{bmatrix},\ g(x) = \begin{bmatrix} 0 \\ -1/a \\ 0 \\ (a+b)/(ab) \end{bmatrix}, \quad (14)$$

where x_1 and x_3 are measured angles (positions), x_2 and x_4 their time derivatives (unmeasured angular velocities), respectively, $a = (m_{l1}l_{c1}^2 + l_r^2 m_{l2} + I_{l1})/\tau$, $b = I_{l2}/\tau$, $c = (m_{l1}l_{c1} + l_r m_{l2}/\tau$, $m_{l1} = 0.2164$kg, $l_r = 0.127$m, $l_{c1} = 0.1173$m, $m_{l2} = 0.085$kg, $I_{l1} = 2.225 \times 10^{-4}$kg·m^2, $I_{l2} = 24.9526 \times 10^{-6}$kg·m^2, $\tau = 0.049443$N· m/V, $g = 9.804$m/s^2. The upright position corresponds to $x_1 = x_2 = 0$.

Since x_1 is the underactuated position, we adopt $y = x_1$ to find a diffeomorphism (2); thus, $\xi_1 = h(x) = x_1$ and $\xi_2 = L_f h(x) = x_2$ follow from the system definitions while

$\eta_1 = \phi_1(x) = x_3$ and $\eta_2 = \phi_2(x) = x_4/a + (a+b)x_2/(ab)$ are proposed to hold $(\partial\phi_i/\partial x)g(x) = 0$ for $i \in \{1,2\}$, i.e.,

$$z = T(x) = \begin{bmatrix}\eta_1\\ \eta_2\\ \xi_1\\ \xi_2\end{bmatrix} = \begin{bmatrix} x_3 \\ \dfrac{x_4}{a} + \dfrac{(a+b)x_2}{ab} \\ x_1 \\ x_2 \end{bmatrix}$$

allows writing the normal form

$$\begin{bmatrix}\dot\eta_1\\ \dot\eta_2\\ \dot\xi_1\\ \dot\xi_2\end{bmatrix} = \begin{bmatrix} a\eta_2 - \dfrac{a+b}{ab}\xi_2 \\ -\dfrac{cg\sin\xi_1}{ab} \\ \xi_2 \\ -\dfrac{u+cg\sin\xi_1}{a} \end{bmatrix}. \tag{15}$$

In order to apply Theorem 3 it is necessary to arrange (15) in the form (3)-(4), where $z_1 \equiv [\eta_1\ \eta_2\ \xi_1]^T$, $z_2 \equiv \xi_2$, in order to identify terms A_{11}, A_{12}, A_{21}, A_{22}, B_2, $f_u(z)$, and $f_m(z)$, i.e.,

$$A_{11} = \begin{bmatrix}0 & 0.0924393 & 0\\ 0 & 0 & 153774.0\\ 0 & 0 & 0\end{bmatrix}, A_{12} = \begin{bmatrix}-184.166\\ 0\\ 1\end{bmatrix},$$

$$A_{21} = [0\ 0\ 77.606],\ A_{22} = 0,\ B_2 = -\frac{1}{a}$$

$$f_u(z) = \begin{bmatrix} a\eta_2 - \dfrac{a+b}{ab}\xi_2 \\ -\dfrac{cg\sin\xi_1}{ab} \\ \xi_2 \end{bmatrix} - A_{11}z_1 - A_{12}z_2,$$

$$f_m(z) = -\frac{cg\sin\xi_1}{a} - A_{21}z_1 - A_{22}z_2.$$

3.2 Double pendulum

The double pendulum, also known as Pendubot, consists of two links, where only that at the base is actuated by means of a DC motor; its model in the form (1) is given by

$$f(x) = \begin{bmatrix} x_2 \\ f_2(x) \\ x_4 \\ f_4(x)\end{bmatrix}, g(x) = \begin{bmatrix} 0 \\ \delta p_2 \\ 0 \\ -\delta(p_2 + p_3\cos x_3)\end{bmatrix}, \tag{16}$$

where x_1 and x_3 are the angular positions of the actuated and underactuated links, respectively, x_2 and x_4 their corresponding angular velocities, $f_2(x) = \delta(p_2 + p_3\cos x_3)(p_3x_2^2\sin x_3 - gp_5(\sin x_3\cos(\pi/2 - x_1) + \sin(\pi/2 - x_1)\cos x_3)) + \delta p_2(p_3x_4^2\sin x_3 + 2p_3x_2x_4\sin x_3 + gp_4\sin(\pi/2 - x_1)) + gp_5(\sin x_3\cos(\pi/2 - x_1) + \sin(\pi/2 - x_1)\cos x_3)$, $f_4(x) = -\delta(p_2 + p_3\cos x_3)(p_3x_4^2\sin x_3 + 2p_3x_2x_4\sin x_3 + gp_4\sin(\pi/2 - x_1) + gp_5\sin x_3\cos(\pi/2 - x_1) + \sin(\pi/2 - x_1)\cos x_3) - \delta(p_3x_2^2\sin x_3 - gp_5(\sin x_3\cos(\pi/2 - x_1) + \sin(\pi/2 - x_1)\cos x_3))(p_1 + p_2 + 2p_3\cos x_3)$, $\delta = 1/(p_2(p_1 + p_2 + 2p_3\cos(x_3)) - (p_2 + p_3\cos(x_3))^2)$, $p_1 = 0.0761$, $p_2 = 0.0662$, $p_3 = 0.0316$, $p_4 = 0.9790$, $p_5 = 0.3830$ y $g = 9.81m/s^2$. The upright position corresponds to $x_1 = x_3 = 0$.

Taking $y = x_3$ (the underactuated position), a diffeomorphism (2) can be found where $\xi_1 = h(x) = x_3$ and $\xi_2 = L_fh(x) = x_4$ follow directly from the system definitions, while $\eta_1 = \phi_1(x) = x_1$ and $\eta_2 = \phi_2(x) = -(p_2 + p_3\cos x_3)x_2 - p_2x_4$ are proposed to hold $(\partial\phi_i/\partial x)g(x) = 0$ for $i \in \{1,2\}$, i.e.,

$$z = T(x) = \begin{bmatrix}\eta_1\\ \eta_2\\ \xi_1\\ \xi_2\end{bmatrix} = \begin{bmatrix} x_1 \\ -(p_2 + p_3\cos x_3)x_2 - p_2x_4 \\ x_3 \\ x_4 \end{bmatrix}.$$

The transformed system is in the normal form

$$\begin{bmatrix}\dot\eta_1\\ \dot\eta_2\\ \dot\xi_1\\ \dot\xi_2\end{bmatrix} = \begin{bmatrix} -(\eta_2 + p_2\xi_2)/(p_2 + p_3\cos\xi_1) \\ c_1 \\ \xi_2 \\ c_2 \end{bmatrix}, \tag{17}$$

where $c_1 = -gp_5\sin(\eta_1 + \xi_1) + (p_3\sin\xi_1(\eta_2 + p_2\xi_2)^2)/(p_2 + p_3\cos\xi_1)^2 - (p_3\xi_2\sin\xi_1(\eta_2 + p_2\xi_2))/(p_2 + p_3\cos\xi_1)$, $c_2 = (2up_2 + 2up_3\cos\xi_1 + p_3^2\xi_2^2\sin 2\xi_1 + 2p_2p_3\xi_2^2\sin\xi_1 - 2gp_1p_5 \times \sin(\eta_1 + \xi_1) + gp_3p_4\sin(\eta_1 + \xi_1) + 2gp_2p_4\sin\eta_1 - gp_3p_5\sin\eta_1 + gp_3p_4\sin(\eta_1 - \xi_1) - gp_3p_5\sin(\eta_1 + 2\xi_1) + (2p_3^2\sin 2\xi_1)(\eta_2 + p_2\xi_2)^2)/(p_2 + p_3\cos^2\xi_1 + (2p_1p_3\sin\xi_1(\eta_2 + p_2\xi_2)^2)/(p_2 + p_3\cos\xi_1)^2 + (2p_2p_3\sin\xi_1(\eta_2 + p_2\xi_2)^2)/(p_2 + p_3\cos\xi_1)^2 - (2p_3^2\xi_2\sin 2\xi_1(\eta_2 + p_2\xi_2))/(p_2 + p_3\cos\xi_1) - (4p_2p_3\xi_2\sin\xi_1 \times (\eta_2 + p_2\xi_2))/(p_2 + p_3\cos\xi_1))$

Theorem 3 requires linking the different terms in (3)-(4) with those in (17); this leads to $z_1 = [\eta_1\ \eta_2\ \xi_1]^T$, $z_2 = \xi_2$, and

$$A_{11} = \begin{bmatrix}0 & 10.2249 & 0\\ 3.7572 & 0 & -3.7572\\ 0 & 0 & 0\end{bmatrix},\ A_{12} = \begin{bmatrix}0.6769\\ 0\\ 1\end{bmatrix},$$

$$A_{21} = [132.3551\ 0\ 100.1801],\ A_{22} = 0,\ B_2 = -24.2124$$

$$f_u(z) = \begin{bmatrix} -\dfrac{\eta_2 + p_2\xi_2}{p_2 + p_3\cos\xi_1} \\ c_1 \\ \xi_2 \end{bmatrix} - A_{11}z_1 - A_{12}z_2,$$

$$f_m(z,u) = c_2 - A_{21}z_1 - A_{22}z_2 - B_2u.$$

3.3 Rotational pendulum

The standard model of the rotational pendulum (also known as the Furuta pendulum) is:

$$f(x) = \begin{bmatrix} x_2 \\ f_2(x) \\ x_4 \\ f_4(x)\end{bmatrix}, g(x) = \begin{bmatrix} 0 \\ g_2(x) \\ 0 \\ g_4(x)\end{bmatrix}, \tag{18}$$

where x_1 and x_3 are the angular positions of the actuated and underactuated links, respectively, x_2 and x_4 their corresponding angular velocities, $f_2(x) = (\beta + \gamma)(\delta x_4^2\sin x_3 - 2\beta x_2x_4\cos x_3\sin x_3)\delta\cos x_3(\beta x_2^2\cos x_3 \times \sin x_3 + \sigma g\sin x_3)/((\beta + \gamma)\beta + \delta^2)\sin^2 x_3 + (\beta + \gamma)\alpha - \delta^2$, $f_4(x) = (\beta\sin^2 x_3 + \alpha)(\beta x_2^2\cos x_3\sin x_3 + \sigma g\sin x_3) - \delta\cos x_3(\delta x_4^2\sin x_3 - 2\beta x_2x_4\cos x_3\sin x_3)/((\beta + \gamma)\beta + \delta^2)\sin^2 x_3 + (\beta + \gamma)\alpha - \delta^2$, $g_2(x) = (\beta + \gamma)/((\beta + \gamma)\beta + \delta^2)\sin^2 x_3 + (\beta + \gamma)\alpha - \delta^2$, $g_4(x) = -(\delta\cos x_3)/((\beta +$

$\gamma)\beta+\delta^2)\sin^2 x_3+(\beta+\gamma)\alpha-\delta^2$, $\alpha=(J_0+m_1L_0^2)/T_c$, $\beta=m_1l_1^2/T_c$, $\gamma=J_1/T_c$, $\delta=m_1L_0l_1/T_c$, $\sigma=m_1l_1/T_c$, $L_0=0.068$m, $J_0=8.4961\times10^{-5}$, $m_1=0.0239$ kg, $l_1=0.0822$, $J_1=1.8281\times10^{-4}$, $T_c=0.004941$, $g=9.81$ m/s^2. The upright position corresponds to $x_1=x_3=0$.

As before, the underactuated position $y=x_3$ is employed to define a diffeomorphism of the form (2), e.g.

$$z=T(x)=\begin{bmatrix}\eta_1\\ \eta_2\\ \xi_1\\ x_2\end{bmatrix}=\begin{bmatrix}x_1\\ \dfrac{x_2\cos(x_3)}{\beta+\gamma}+\dfrac{x_4}{\delta}\\ x_3\\ x_4\end{bmatrix},$$

based on which the normal form

$$\begin{bmatrix}\dot\eta_1\\ \dot\eta_2\\ \dot\xi_1\\ \dot\xi_2\end{bmatrix}=\begin{bmatrix}(\eta_2-\xi_2/\delta)\,(\beta+\gamma)/\cos\xi_1\\ d_1\\ \xi_2\\ d_2\end{bmatrix},\qquad(19)$$

is obtained, where $d_1=-(\sin\xi_1(\beta^3(\eta_2-(\xi_2/\delta))^2\cos^3\xi_1-\beta^3(\eta_2-(\xi_2/\delta))^2\cos\xi_1-\beta^2g\sigma-\alpha g\gamma\sigma-\beta g\gamma\sigma-\alpha\beta^2(\eta2-(\xi_2/\delta))^2\times\cos\xi_1+\beta^2g\sigma\cos^2\xi_1-\beta^2\gamma(\eta_2-(\xi_2/\delta))^2\cos\xi_1-\delta^3(\eta_2-(\xi_2/\delta))\xi_2\cos^2\xi_1+\beta^2\delta(\eta_2-(\xi_2/\delta))\xi_2+\beta^2\gamma(\eta_2-(\xi_2/\delta))^2\times\cos^3\xi_1+\beta^2\delta^2(\eta_2-(\xi_2/\delta))^2\cos^3\xi_1-\alpha\beta g\sigma-\alpha\beta\gamma(\eta_2-(\xi_2/\delta))^2\cos\xi_1+\beta g\gamma\sigma\cos^2\xi_1+\alpha\beta\delta(\eta_2-(\xi_2/\delta))\xi_2+\alpha\delta\gamma(\eta_2-(\xi_2/\delta))\xi_2+\beta\delta\gamma(\eta_2-(\xi_2/\delta))\xi_2+\beta\delta^2g\sigma\cos^2\xi_1+\delta^2g\gamma\sigma\cos^2\xi_1-\beta^2\delta(\eta_2-(\xi_2/\delta))\xi_2\cos^2\xi_1+\beta\delta^2\gamma(\eta_2-(\xi_2/\delta))^2\cos^3\xi_1-\beta\delta\gamma(\eta_2-(\xi_2/\delta))\xi_2\cos^2\xi_1)/(\delta(\beta+\gamma)(\alpha\beta+\alpha\gamma+\beta\gamma-\beta^2\cos^2\xi_1-\delta^2\cos^2\xi_1+\beta^2-\beta\gamma\cos^2\xi_1))$, $d_2=(\beta^2(\eta_2-(\xi_2/\delta))^2\sin2\xi_1-2\delta u\cos\xi_1-\delta^2\xi_2^2\sin2\xi_1-2\beta^2(\eta_2-(\xi_2/\delta))^2\cos^3\xi_1\sin\xi_1+\alpha\beta(\eta_2-(\xi_2/\delta))^2\sin2\xi_1+2\alpha g\sigma\sin\xi_1+2\beta g\sigma\sin^3\xi_1+4\beta\delta(\eta_2-(\xi_2/\delta))\xi_2\sin\xi_1-4\beta\delta(\eta_2-(\xi_2/\delta))\xi_2\sin^3\xi_1)/(2(\alpha\beta+\alpha\gamma+\beta\gamma-\beta^2\cos^2\xi_1-\delta^2\cos^2\xi_1+\beta^2-\beta\gamma\cos^2\xi_1))$.

Identifying the different terms in (19) that allow applying Theorem 3 we have $z_1=[\eta_1\ \eta_2\ \xi_1]^T$, $z_2=\xi_2$, and

$$A_{11}=\begin{bmatrix}0&0.069652&0\\0&0&2071.2\\0&0&0\end{bmatrix},\ A_{12}=\begin{bmatrix}-2.5772\\0\\1\end{bmatrix},$$

$$A_{21}=[0\ 0\ 76.176],\ A_{22}=0,\ B_2=-13.3526$$

$$f_u(z)=\begin{bmatrix}(\eta_2-\xi_2/\delta)\,(\beta+\gamma)/\cos\xi_1\\ d_1\\ \xi_2\end{bmatrix}-A_{11}z_1-A_{12}z_2,$$

$$f_m(z,u)=d_2-A_{21}z_1-A_{22}z_2-B_2u.$$

4. SIMULATION AND REAL-TIME IMPLEMENTATIONS

The results of implementing the control laws developed in the previous section are shown in the sequel. Simulations do not consider the control magnitude of (8)-(9) as a limitation; on the other hand, real-time implementations require taking into account the maximum voltage allowed for the single DC motor in the Mechatronics Kit, i.e., LMI-based gains such as M and γ_2 in the discontinuous term ρ should be tuned as to hold the input constraint $\bar u$. The LMI framework allows for such constraints to be automatically incorporated in the calculation of the gains; see (Bernal et al., 2022, Section 5.6.1). Moreover, since angular velocities are not available in real time, they should be estimated by means of a Levant's robust differentiator; to this end, a 10th-order differentiator has been employed even if only the first time derivative is need, since precision gets better as the order increases [1].

Inertia pendulum: Figure 2 shows the simulation results of implementing the control law (8)-(9) with A_{11}, A_{12}, A_{21}, A_{22}, B_2, $f_u(z)$, $f_m(z)$ as defined in Section 3.1, and $\Phi=-10$, $\Lambda=1$, $P_2=1/20$, $\gamma_2=10$, $M=[0.0028\ 0.0002\ 11.5182]$ as deduced from LMIs and relationships in Theorem 3. The underactuated angle x_1 (top) and its corresponding angular velocity x_2 (middle) reach the desired position of 0 by means of the control law u (bottom); logarithmic time scale has been employed to clearly distinguish the signals in the transient. Similarly,

[1] Videos of the real-time implementations are available at `https://drive.google.com/drive/folders/1OqeKnnERvFjCWy59fV6rUbNmHbGHg_AG?usp=drive_link`.

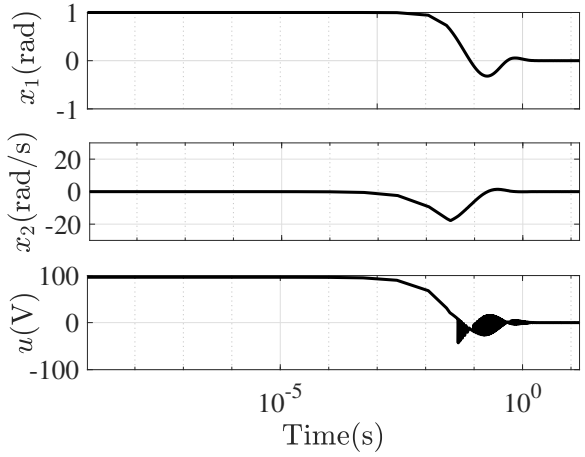

Fig. 2. Inertia pendulum in simulation

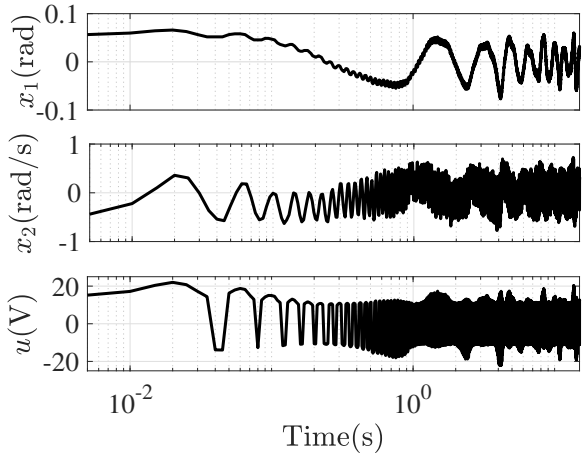

Fig. 3. Inertia pendulum in real-time implementation

Figure 3 shows the real-time results of implementing the control law designed for simulation; no adjustments were required, except for the initial condition being taken close enough to the reference. Oscillations at the end are the result of discontinuous control action as well as the differentiator precision.

Double pendulum (Pendubot): Figure 4 shows the simulation results of implementing the control law (8)-(9) with A_{11}, A_{12}, A_{21}, A_{22}, B_2, $f_u(z)$, $f_m(z,u)$ as defined in Section 3.2, and $\Phi = -10$, $\Lambda = 1$, $P_2 = 1/20$, $\gamma_2 = 200$, $M = [-246.7677\ -384.2139\ 203.0371]$, $\bar{u} = 100$. Recall that simulation does not consider any control magnitude bound (bottom) which clearly exhibits discontinuous behaviour; positions of the actuated link x_1 (top) and the underactuated link x_3 (middle) are shown. Real-time results are shown in Figure 5, where the voltage constraints had to be respected by tuning the controller parameters $\gamma_2 = 20$ and $M = [-54.8844\ -90.1329\ 52.15139]$; again, oscillations get higher as the control law switches at higher frequencies.

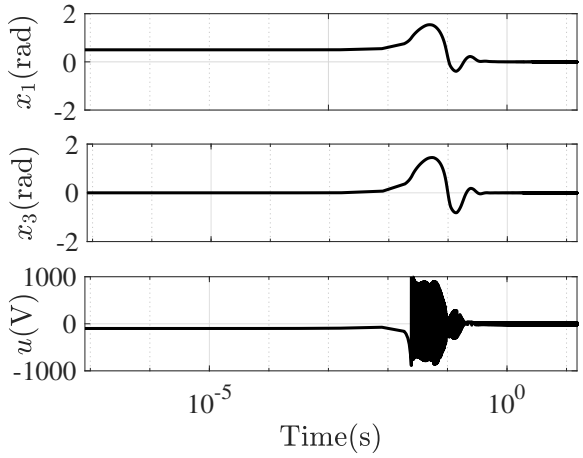

Fig. 4. Double pendulum in simulation

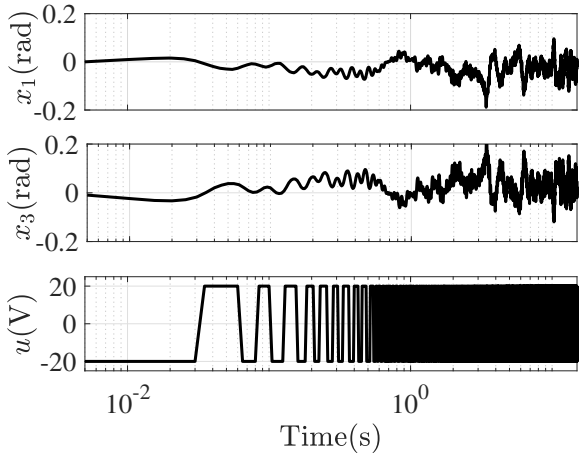

Fig. 5. Double pendulum in real-time implementation

Rotational pendulum (Furuta): Figure 6 shows the simulation results of implementing the control law (8)-(9) with A_{11}, A_{12}, A_{21}, A_{22}, B_2, $f_u(z)$, $f_m(z,u)$ as defined in Section 3.3, and $\Phi = -0.5$, $\Lambda = 1$, $P_2 = 1$, $\gamma_2 = 100$, $M = [72.1631\ 284.4638\ 187.0222]$. The underactuated angle x_3 (top) and its corresponding angular velocity x_4 (middle) are driven to 0 by means of the discontinuous control law u (bottom). For real-time implementation, the magnitude of the control signal in simulation is unacceptable; therefore, parameters are tuned to new values $\gamma_2 = 20$ and $M = [0.4159\ 0.0227\ 13.0719]$ as to obtain the results in Figure 7. For the sake of illustration, some gains of the Levant's robust differentiator are given: $\lambda_0 = 150$, $\lambda_1 = 93$, $\lambda_2 = 58$, $\lambda_3 = 36$, $\lambda_4 = 22$ $\lambda_5 = 11$, $\lambda_6 = 8$, $\lambda_7 = 5$, $\lambda_8 = 3$, $\lambda_9 = 2$, $\lambda_{10} = 1.1$.

5. CONCLUSION

A novel LMI-based sliding mode control scheme based on the unit vector approach and a diffeomorphism leading to the normal form, has been presented. The proposal has

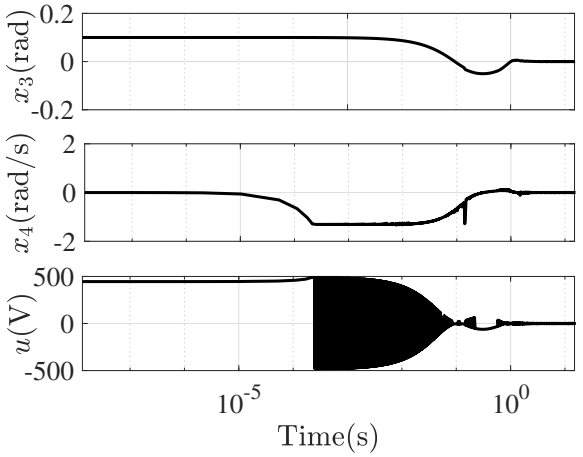

Fig. 6. Rotational pendulum in simulation

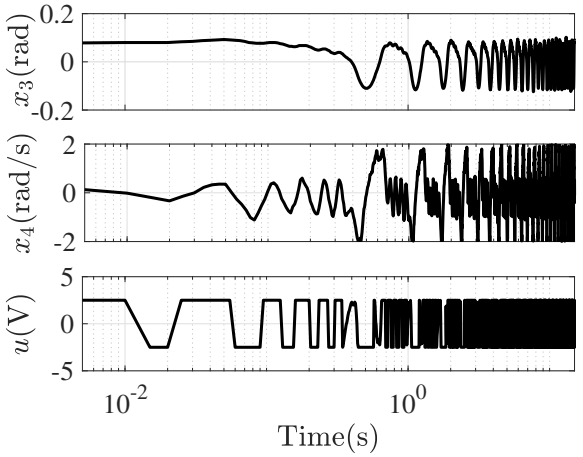

Fig. 7. Rotational pendulum in real time

been successfully put at test in a variety of underactuated configurations of a mechatronics kit (rotational, inertia, and double pendulum), both in simulation and real-time, with enough detail as to reproduce the obtained results. Future work on more specific sliding mode control schemes addressed to underactuated systems is under course.

REFERENCES

Angeli, D. (2001). Almost global stabilization of the inverted pendulum via continuous state feedback. *Automatica*, 37(7), 1103–1108.

Ashari, A.E. (2004). Sliding-mode control of active suspension systems: unit vector approach. In *Proceedings of the 2004 IEEE International Conference on Control Applications, 2004.*, volume 1, 370–375. IEEE.

Begovich, O., Sanchez, E.N., and Maldonado, M. (2002). Takagi-Sugeno fuzzy scheme for real-time trajectory tracking of an underactuated robot. *IEEE Transactions on Control Systems Technology*, 10(1), 14–20.

Bernal, M., Sala, A., Lendek, Z., and Guerra, T.M. (2022). *Analysis and Synthesis of Nonlinear Control Systems*. Springer.

Boyd, S., Ghaoui, L.E., Feron, E., and Belakrishnan, V. (1994). *Linear Matrix Inequalities in System and Control Theory*, volume 15. SIAM: Studies In Applied Mathematics, Philadelphia, USA.

Capriotti, E. and Marti-Renom, M.A. (2008). Rna structure alignment by a unit-vector approach. *Bioinformatics*, 24(16), i112–i118.

Edwards, C. and Spurgeon, S. (1998). *Sliding mode control: theory and applications*. Taylor and Francis Ltd., UK, Padstow, UK.

Farwig, M., Zu, H., and Unbehauen, H. (1990). Discrete computer control of a triple-inverted pendulum. *Optimal Control Applications and Methods*, 11(2), 157–171.

Fliegner, T. and Smith, M. (1998). On the robustness of continuously approximated sliding mode schemes. *IFAC Proceedings Volumes*, 31(17), 237–242.

Furuta, K., Kajiwara, H., and Kosuge, K. (1980). Digital control of a double inverted pendulum on an inclined rail. *International Journal of control*, 32(5), 907–924.

Furuta, K., Yamakita, M., and Kobayashi, S. (1992). Swing-up control of inverted pendulum using pseudo-state feedback. *Proceedings of the Institution of Mechanical Engineers, Part I: Journal of Systems and Control Engineering*, 206(4), 263–269.

Gahinet, P., Nemirovski, A., Laub, A.J., and Chilali, M. (1995). *LMI Control Toolbox*. Math Works, Natick, USA.

Hajkarami, H., Ahmadi, M.S., and Danesh, M. (2010). Unit vector approach based sliding mode control of a small-scale unmanned helicopter. In *IEEE ICCA 2010*, 28–33. IEEE.

Hernández, V.M. (2003). A combined sliding mode-generalized pi control scheme for swinging up and balancing the inertia wheel pendulum. *Asian Journal of Control*, 5(4), 620–625.

Izutsu, M., Pan, Y., and Furuta, K. (2008). Swing-up of furuta pendulum by nonlinear sliding mode control. *SICE Journal of Control, Measurement, and System Integration*, 1(1), 12–17.

Khalid, N. and Memon, A.Y. (2014). Output feedback stabilization of an inertia wheel pendulum using sliding mode control. In *2014 UKACC International Conference on Control (CONTROL)*, 157–162. IEEE.

Khalil, H. (2014). *Nonlinear Control*. Prentice Hall, New Jersey, USA.

Lee, T.B. and Yang, H.S. (2009). Sliding surface design by eigenstructure assignment and sliding mode control of matched uncertain systems. *Journal of Institute of Control, Robotics and Systems*, 15(8), 812–817.

Levant, A. (2003). Higher-order sliding modes, differentiation and output-feedback control. *International journal of control*, 76(9-10), 924–941.

Quanser (2006). Mechatronics control kit user's manual. kit manual.

Ryan, E. and Corless, M. (1984). Ultimate boundedness and asymptotic stability of a class of uncertain dynamical systems via continuous and discontinuous feedback control. *IMA journal of mathematical control and information*, 1(3), 223–242.

Spong, M.W., Corke, P., and Lozano, R. (2001). Nonlinear control of the reaction wheel pendulum. *Automatica*, 37(11), 1845–1851.

Sun, N., Fang, Y., and Chen, H. (2015). A novel sliding mode control method for an inertia wheel pendulum system. In *2015 International Workshop on Recent Advances in Sliding Modes (RASM)*, 1–6. IEEE.

Van Kien, C., Son, N.N., and Anh, H.P.H. (2016). A stable lyapunov approach of advanced sliding mode control for swing up and robust balancing implementation for the pendubot system. In *AETA 2015: Recent Advances in Electrical Engineering and Related Sciences*, 411–425. Springer.

Wadi, A., Lee, J.H., and Romdhane, L. (2018). Nonlinear sliding mode control of the furuta pendulum. In *2018 11th International Symposium on Mechatronics and its Applications (ISMA)*, 1–5. IEEE.

Xu, J., Niu, Y., Lim, C.C., and Shi, P. (2020). Memory output-feedback integral sliding mode control for furuta pendulum systems. *IEEE Transactions on Circuits and Systems I: Regular Papers*, 67(6), 2042–2052.

Yoo, D.S. (2013). Balancing control for the pendubot using sliding mode. In *IEEE ISR 2013*, 1–4. IEEE.

Zehar, D. and Benmahammed, K. (2013). Optimal sliding mode control of the pendubot. *Int. Research J. of Computer Sci. and Information Syst.(IRJCSIS)*, 2(3), 45–51.